Technical Note

Feature Extraction for Moving Targets Based on the Statistical Characteristics of Echo Amplitude with the L-Band Fully Polarimetric Radar

Chuang Zhang [1], Yaxin Mu [2], Zhenghuan Xia [1], Shichao Jin [1], Fuzhan Yue [1], Xin Liu [1,*], Lanqing Zhang [3], Zhixin Tian [4], Zongqiang Liu [1], Yao Zhang [1], Wenning Gao [1], Tao Zhang [1], Zhilong Zhao [1] and Ying Zhang [1]

1   State Key Laboratory of Space-Ground Integrated Information Technology, Beijing Institute of Satellite Information Engineering, Beijing 100095, China
2   School of Information and Communication Engineering, Beijing Information Science and Technology University, Beijing 100101, China
3   China Spacesat Company Limited, Beijing 100095, China
4   Beijing Institute of Spacecraft System Engineering, China Academy of Space Technology, Beijing 100095, China
*   Correspondence: liuxin115@foxmail.com

Abstract: Non-imaging radar can achieve the detection and localization of moving targets, but it faces difficulties in the classification of targets. Aiming for the application of moving target classification by low/medium resolution non-imaging radar, this paper proposes a novel feature extraction method, based on the statistical characteristics of echo amplitude with the L-band fully polarimetric radar. A feature plane, composed of the 3rd-order central moment (skewness) and 4th-order central moment (kurtosis) as the statistical characteristics of the echo envelope, is established. In addition, two types of moving targets, pedestrians and non-motorized vehicles, are able to be effectively distinguished according to whether the echo signals of different polarizations have overlapping areas in the feature plane. The L-band fully polarimetric radar has been developed and field experiments have been conducted. The experimental results verify that the kurtosis and skewness of the fully polarimetric echo amplitude of the pedestrians are very close, and there is an overlapping area in the feature plane, while the statistical characteristics of the fully polarimetric echo signal of non-motor vehicles are different, and there is no overlapping area in the feature plane. This proposed feature extraction method has the advantage of being simple and robust, compared to the traditional imaging approach.

Keywords: L-band fully polarimetric radar; statistical characteristics; central moment; target feature extraction

1. Introduction

Non-imaging radar is able to detect and locate the moving target, which is widely used in missile warning, aerial vehicle tracking, satellite tracking, etc. [1–3]. However, the classification of the moving target is facing challenges, and it is worth devoting effort to classifying moving targets using low/medium resolution non-imaging radar.

Radar Target Recognition (RTR) is based on the analysis of the electromagnetic scattering mechanism of the target. Collecting the radar echo signals, generated by the interested targets, and extracting information such as amplitude, phase, spectrum, polarization, and various statistical features, is used to identify the types and attributes of targets. The distribution of scattering centers of a target along the line of sight of radar is featured by the high resolution range profile (HRRP), reflecting the important characteristics of the target [4,5]. In addition, the polarization information is closely related to the surface roughness, symmetry, orientation, and other characteristics of the scattering components in the target distance unit.

Recently, RATR technology, based on fully polarimetric HRRP, has attracted increasing attention [6–13]. In [6], the incoherent decomposition method is proposed to extract the

scattering entropy, scattering angle, and anisotropy characteristics along the radial distance of multiple types of aircraft under different scales. Reference [7] designed a classifier by dynamically combining the skewness, coefficient of variation, and energy cluster length features of a single polarization channel, and the decision-level fusion of the outputs of different classifiers were conducted. Reference [8] studied the polarization invariant characteristics of three types of scatterers, namely cone (a simulated bullet), sphere and cylinder, and simulation experiments were conducted to achieve a classification performance of more than 80% for the three types of targets. According to the geometrical diffraction (Geometric Theory of Diffraction, GTD) model parameters and Krogager decomposition parameters, reference [9] recognized the types of scattering centers contained in the target, and used the density clustering algorithm to classify the targets, achieving the classification of three types of vehicles within a certain angular domain. In addition, there are some other methods that can be used for target classification. For example, in reference [10], super-resolution mapping, based on a spatial–spectral correlation for spectral Imagery, is proposed to improve the accuracy of the land-cover class. In addition, the paper used an object-based approach in multitemporal SAR flood images to improve the pixel-based change detection accuracy [11].

It is noted that the existing target recognition methods mostly require the acquisition of high-resolution polarimetric radar echo signals, which imposes high demands on the radar system. The low-resolution polarimetric echo signal has less local scattering characteristics for the target than the high-resolution polarimetric echo signal, and more ambiguity in the polarimetric description parameters. Based on low-resolution polarimetric echoes, this paper proposes a novel feature extraction method, based on the statistical characteristics of the echo amplitude of the fully polarimetric radar echoes.

We have developed an L-band fully polarimetric radar; the processing flow of the radar data is given, and a feature plane, consisting of the 3rd-order and 4th-order central moment of echo envelope, is created. In addition, detection experiments have been conducted for two types of moving targets, pedestrians, and non-motor vehicles, to evaluate the proposed feature extraction algorithm. The experiment results verify that the kurtosis and skewness distributions of the VH, VV, and HH polarized echo signals of pedestrians and non-motorized vehicles are significantly different, achieving the classification of the targets. Compared with the traditional imaging algorithm, this proposed feature extraction method does not need to perform imaging or other complex processing, and the statistical features of the fully polarimetric echo envelope are estimated simply and quickly, greatly reducing the processing time.

The main contributions of this work are as follows. Firstly, the low/medium resolution non-imaging radar is applied to the moving target classification. The L-band fully polarimetric radar is used as a low/medium resolution non-imaging radar. Secondly, the statistical characteristics of the amplitude of the fully polarimetric radar echoes are used as the features of the moving targets. Thirdly, the velocity range for the targets in the proposed extraction method is derived. The velocity is limited by the adjacent phase difference of the targets in the azimuth direction, and the sampling interval in the range direction. Lastly, compared with the traditional polarization decomposition methods, the proposed method is simple and robust. The proposed method utilizes signal detection, while the traditional polarization decomposition methods utilize imaging detection. In addition, this proposed method used the statistical features as the echo signal features.

This paper is organized as follows. Section 2 introduces the components of the L-band fully polarimetric radar system. In Section 3, the radar signal processing flow and the feature extraction method of the moving target are described in detail. Section 4 shows the field experiment and the discussion of the results. The conclusions are given in Section 5.

2. Fully Polarimetric Radar System

Because there is almost no verified L-band full-polarization radar reported in the previous papers, we describe our design in detail in this paper.

2.1. System Design

The L-band fully polarimetric radar has been developed to obtain the fully polarimetric scattering information of the target and have excellent penetration performance. Two pairs of L-band high-gain horn antennas are designed, in which one pair of horn antennas is used to transmit the vertically polarimetric (V) and horizontally polarimetric (H) electromagnetic waves, and the other pair of horn antennas is used to receive the vertically polarimetric (V) and horizontally polarimetric (H) echo signals, simultaneously. Thus, four echoes of VV, VH, HH and HV information of the target can be estimated [14–16].

The main components of the fully polarimetric radar system are shown in Figure 1. It consists of six modules, which are the fully polarimetric horn antenna, radio frequency front-end subsystem, dual-channel signal generator, dual-channel receiver, clock management module, and the radar main control software.
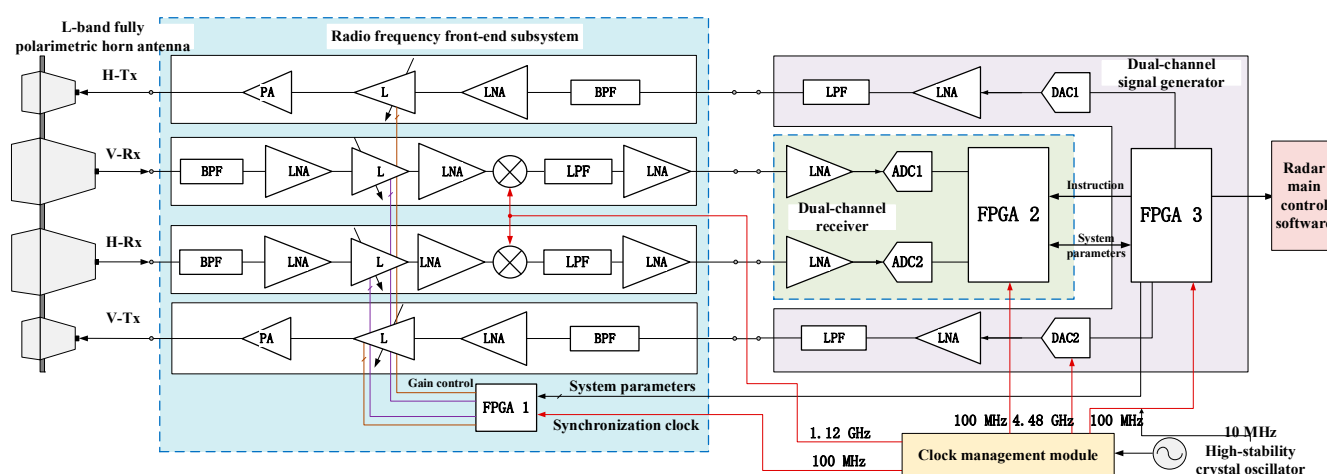

Figure 1. Block diagram of L-band fully polarimetric radar system.

Two pairs of horn antennas are designed for the transmission and reception of L-band fully polarimetric signals. The gain of the transmitting antenna is 10.5 dB, the gain of the receiving antenna is 15.5 dB, and the polarization isolation is better than 31 dB.

The RF front-end subsystem has two functions. Firstly, it amplifies the transmitted signal. Secondly, the radar echo signal is processed by bandpass filtering (BPF), low-noise amplification (LNA), down-conversion and low-pass filtering (LPF) to obtain an intermediate frequency (IF) echo signal. Finally, the center frequency of the IF echo signal is 140 MHz, and the bandwidth is 70 MHz.

The signal generator is able to generate positive and negative sweep signals with a center frequency of 1.26 GHz and a bandwidth of 70 MHz, as demonstrated in Figure 2. The positive and negative sweep signals are orthogonal, which do not interfere with each other, and the echoes can be separated by the matched filters. In addition, the positive and negative sweep signals have the same signal spectrum.

The dual channel radar receiver executes the amplification and quantization of the IF echo signal, acquiring the IF echo signal in the digital domain. The clock management module is able to generate multiple clock signals, such as the synchronization clock, DAC sampling clock, and FPGA working clock. The radar master control software is used to control the system transmission power, receiver gain, sampling window and other parameters. The main parameters of the fully polarimetric radar system are listed in Table 1. The sensitivity of the radar receiver is better than −90 dBm; it is therefore capable of receiving echoes from distant weak targets.
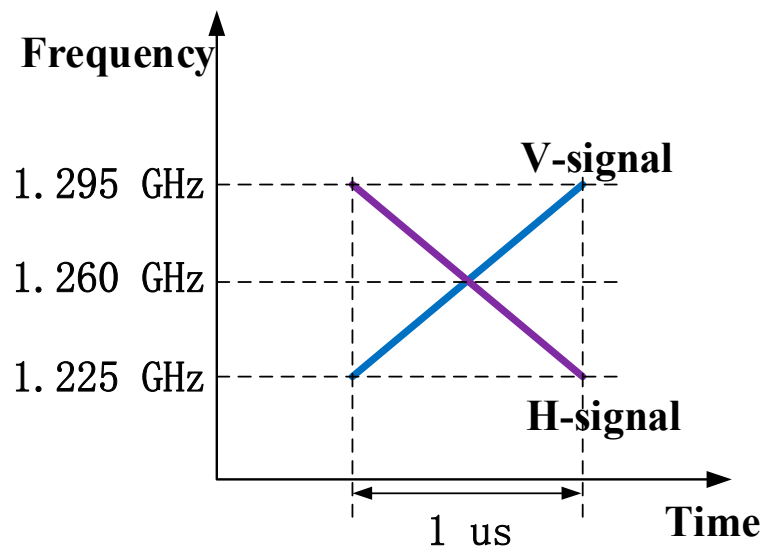
Figure 2. Positive and negative swept linear frequency modulation signal.

Table 1. The main parameters of L-band fully polarimetric radar system.

Indicator	Value
Center frequency	1.26 GHz
Bandwidth	70 MHz
Range resolution	2.14 m
Time interval (width)	1 us
Polarization mode	VV, VH, HV, HH
Transmitted power	10 dBm
Transmit Antenna gain	$\geq$10.5 dB
Receive antenna gain	$\geq$15.5 dB
Sensitivity of receiver	~$-$90 dBm
Sampling rate	200 MSPS
Quantitative bits	16 bit
Power consumption	$\leq$240 W
Weight	$\leq$80 kg

2.2. Fully Polarimetric Radar Echo

The sequence diagram of the fully polarimetric radar is shown in Figure 3. The radar simultaneously transmits positive and negative frequency-modulated Chirp signals with 10 dBm power and 1 us time width, and the receiver synchronously receives the radar echo signal with a time width of 7.5 us. The maximum detection distance is about 1 km.

Figure 4 illustrates the acquisition of fully polarimetric signals. For the transmitter, the V-polarized antenna transmits a positive sweep signal and the H-polarized antenna transmits a negative sweep signal. All echo signals are received by the two polarimetric receiving antennas, and then the baseband signals can be obtained after the orthogonal demodulation. Finally, the output of the positive matched filter is the echo signal emitted by the V-polarized antenna, and the output of the negative matched filter is the echo signal emitted by the H-polarized antenna. Thus, the fully polarimetric radar echoes are collected.
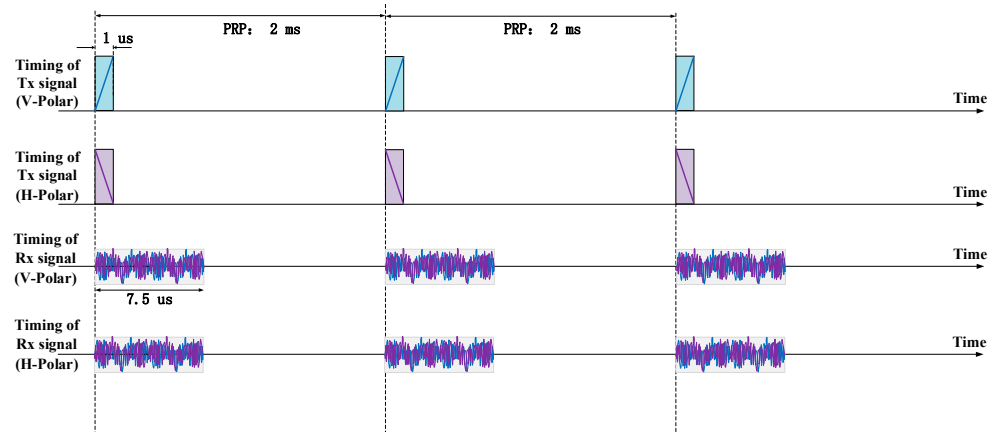
Figure 3. The sequence diagram of the fully polarimetric radar.
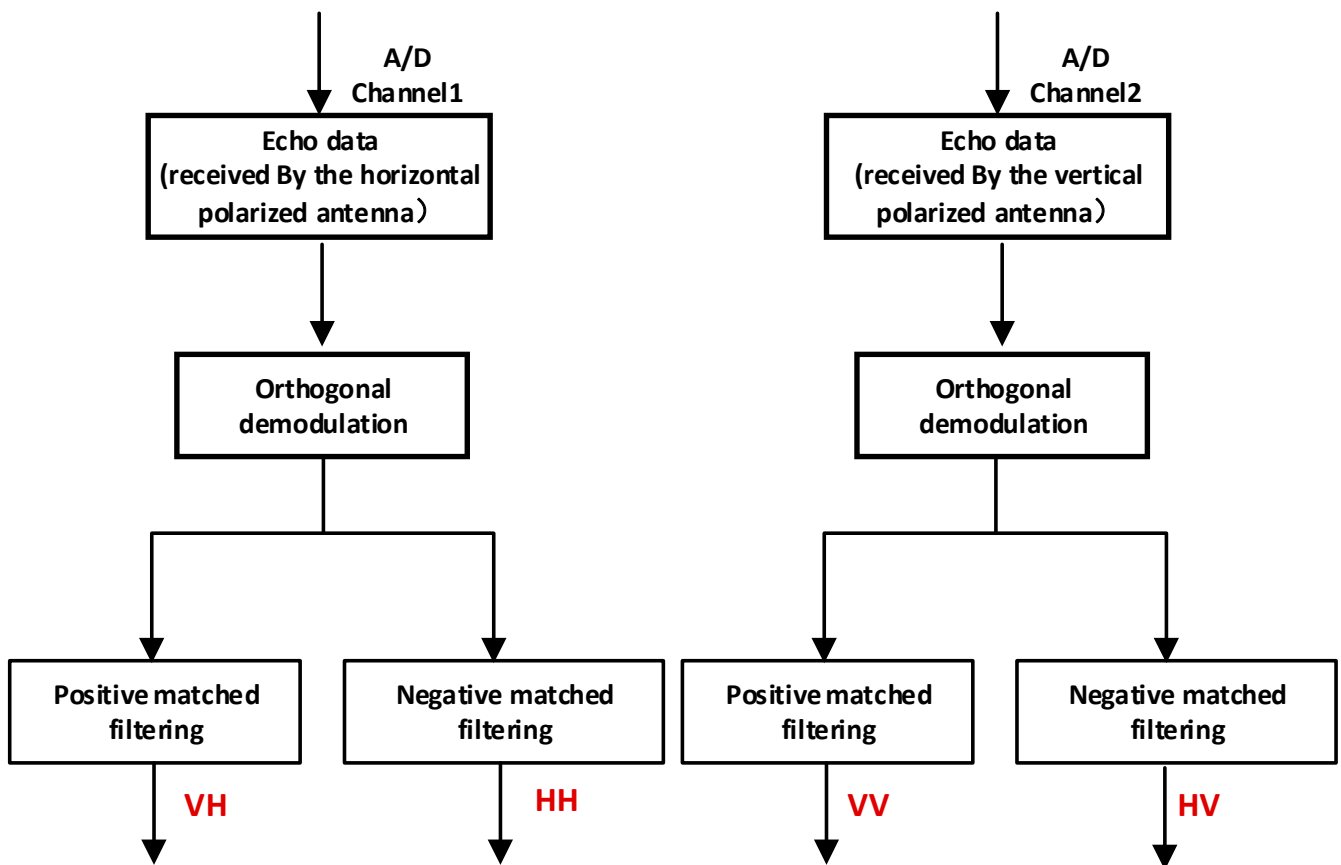

Figure 4. The acquisition of the fully polarimetric radar echo.

3. Feature Extraction Method of Moving Target

3.1. Radar Data Processing Flow

Because of the reciprocity of VH and HV, we only focus on three kinds of polarized data: VH, VV, and HH. The flow chart of the feature extraction method for the moving targets is displayed in Figure 5. The process consists of five main steps:

Step 1: orthogonal demodulation. The baseband signal is obtained after the digital signals corresponding to the two polarized antennas are orthogonally demodulated.

Step 2: matched filtering. For the H-polarized antenna, VH and HH polarization echo signals are acquired through positive and negative matched filters, separately. For

the V-polarized antenna, a VV polarization echo signal is acquired through a positive matched filter.

Step 3: background removal. The influence of background clutter in experiment senses have been eliminated.

Step 4: statistical model. The energy normalization is performed, then the statistical quantities (central moment) of the VH, VV, and HH polarized signals are calculated.

Step 5: statistical feature fusion of multi-polarized echoes. A feature plane is established, and the statistical feature of the VH, VV and HH polarized signals are fused, to distinguish different targets.
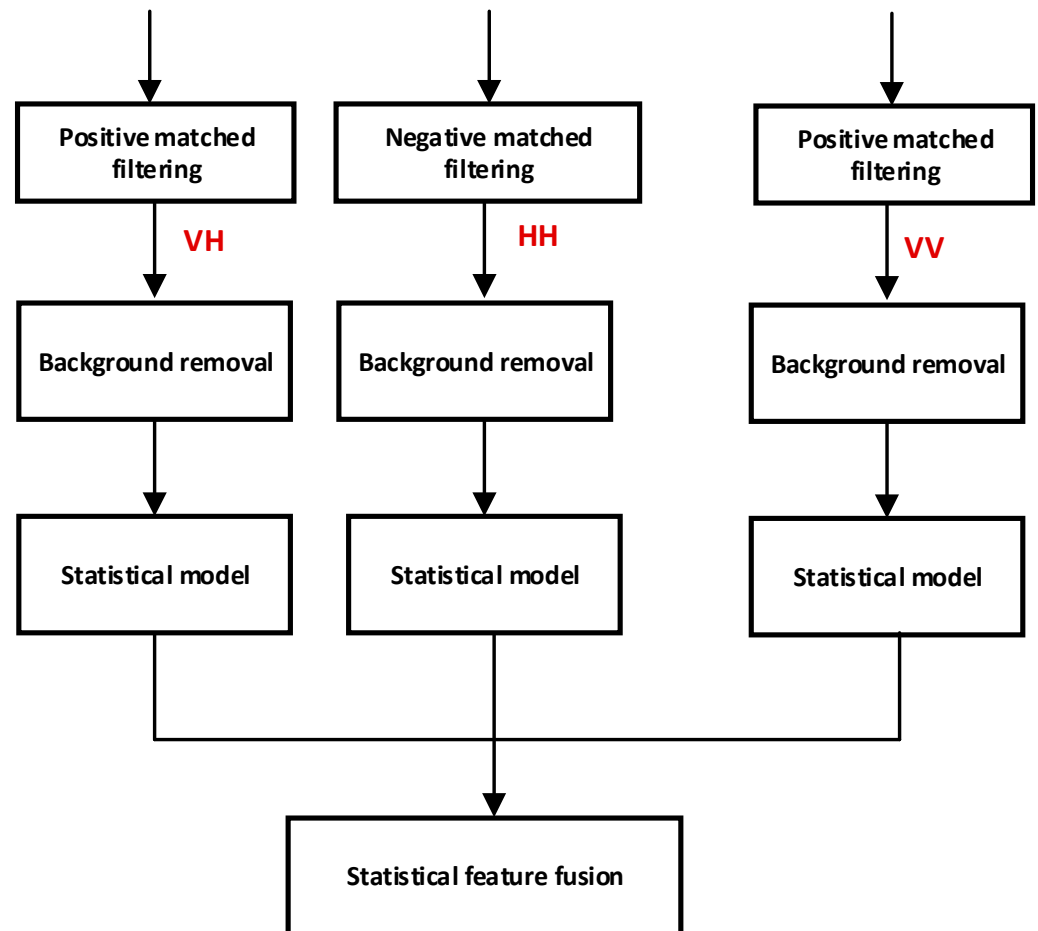
Figure 5. The flow chart of fully polarimetric radar signal processing.

3.2. Background Removal

After orthogonal demodulation and the matching filtering, 2D range profiles can be obtained, as shown in Figure 6a. It is clear that the path of the moving target cannot be observed directly from the original range profiles, because the intensity of the background echo signal is significantly stronger than the scattered signal generated by the moving target. The background echo signal mainly includes the electromagnetic wave directly coupled to the transmitting antenna and the scattered field generated by the stationary target in the detection area. The signal-to-noise ratio (SNR) can be significantly improved after the elimination of the background echo.
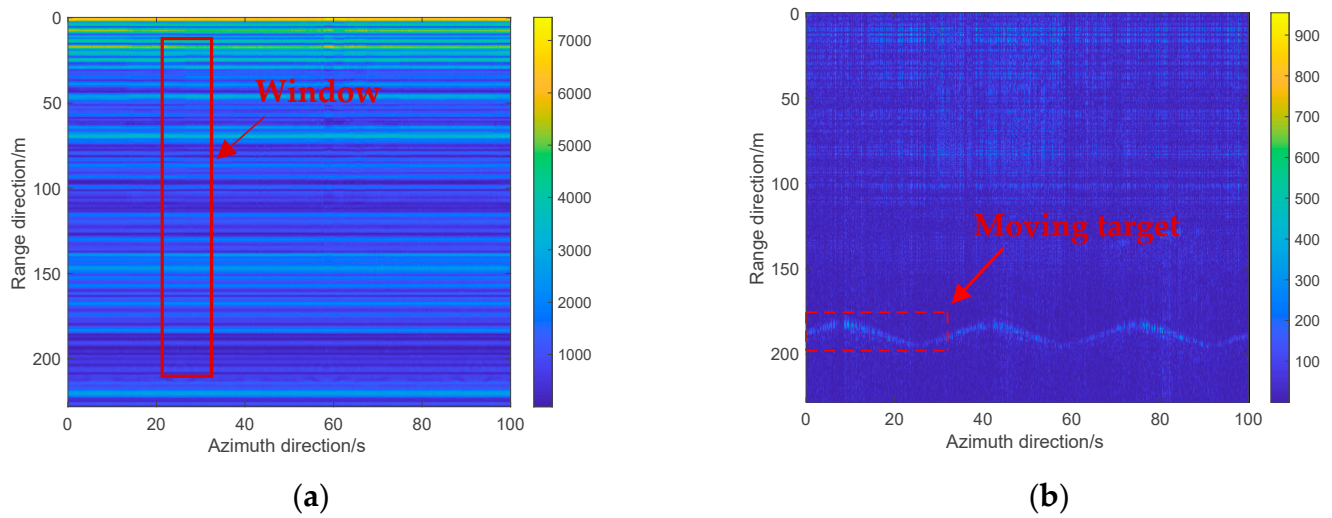
Figure 6. 2D range profiles. (**a**) Before the removal of background. (**b**) After the removal of background.

The echo signal received by the radar is modeled as [17]:

$$x(m,n) = x_M(m,n) + x_B(m,n) + N(m,n). \tag{1}$$

where $x(m,n)$ denotes the strength of the received echo signal, $m = 1, 2, \ldots, M$, denotes the samples in range, $n = 1, 2, \ldots, N$, and denotes the samples in azimuth. $x_M(m,n)$ is the echo generated by the moving target, $x_B(m,n)$ is the echo of the background scattering, and $N(m,n)$ is random noise.

Selecting a window with the length of $N1$ in azimuth, the background scattering signal and noise signal within the window are estimated as:

$$x_B(m) + N(m) \approx \frac{1}{N1} \sum_{n=1}^{N1} x(m,n). \tag{2}$$

Combining (1) and (2), the echo signal of the moving target is calculated as:

$$x_M(m) \approx x(m) - \frac{1}{N1} \sum_{n=1}^{N1} x(m,n). \tag{3}$$

Setting the sliding window until it covers the entire detection area, the echo signal of the target can be separated from the received echo signal. Figure 6b depicts the 2D range profiles after the removal of the background, showing that the trajectory of the moving target is clear and the SNR has been improved.

3.3. Probability Density Function of the Intensity of Radar Echo Signal

The probability density curve of the signal intensity of radar echo in fully polarimetric mode is studied and estimated [18]. Figure 7 demonstrates the estimation process of the probability density curve of the echo intensity.

Firstly, the L-band fully polarimetric radar periodically transmits and receives L-band signals in the detection area, and the detection scene is shown in Figure 7a. After orthogonal demodulation, pulse compression, and background removal, 2D range profiles are obtained, as illustrated in Figure 7b. The probability density function of the echo signal is estimated according to the histogram of the multi-channel echo signal intensity in the sampling window. Figure 7c gives the probability density curve in the sampling window.

(**a**)

(**b**)

(**c**)
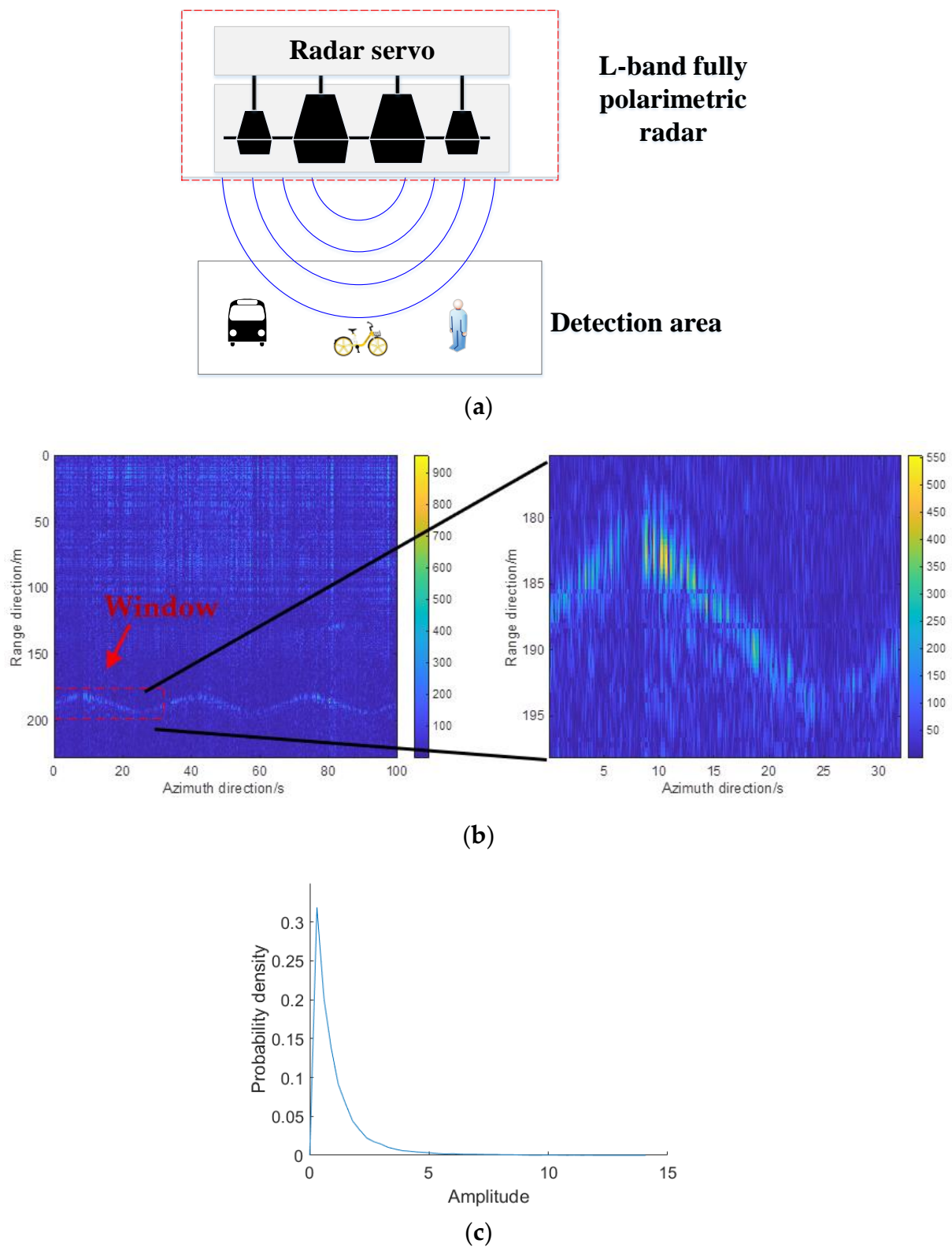
Figure 7. Estimation process of probability density function of radar echo. (**a**) Experiment scene. (**b**) 2D range compressed profile and its sampling window. (**c**) The curve of probability density function.

3.4. Statistical Model

In order to compare the statistical characteristics of different types of targets, the echo signal should be energy normalized before calculating the central moment [19,20]:

$$\hat{x} = \frac{|x|}{\sqrt{E[|x|^2]}},$$

(4)

where x is the strength of the echo signal, $|x|$ is the absolute value of x, $\hat{x}$ is the energy normalized echo signal, and $E[|x|^2]$ is the expectation of $|x|^2$.

The calculation formula of the n-th order central moment is as follows [19]:

$$M_n = E\left[\frac{(\hat{x} - \mu)^n}{\sigma^n}\right],$$

(5)

where μ and σ are the mean and standard deviation of the intensity of the echo signal, respectively.

When $n = 3$, the 3rd-order central moment of the radar echo signal intensity can be obtained according to (5). The 3rd-order central moment is also known as skewness, measuring how differently shaped the tails of the distribution are, in comparison to the tails of the normal distribution, estimated as:

$$M_3 = E\left[\frac{(\hat{x} - \mu)^3}{\sigma^3}\right].$$

(6)

Similarly, when $n = 4$, the 4th-order central moment is estimated as:

$$M_4 = E\left[\frac{(\hat{x} - \mu)^4}{\sigma^4}\right].$$

(7)

The 4th-order central moment is also known as kurtosis, referring to a distortion or asymmetry that deviates from the symmetrical bell curve.

In addition, we derived the velocity range for targets in the proposed extraction method. If the moving target can be detected from the background, the adjacent phase difference of targets in the azimuth direction should be smaller to $\frac{\pi}{8}$, which is estimated as:

$$\frac{2 \times V_R \times 2 \times \pi \times N_a}{\frac{c}{f_c} \times PRF} \geq \frac{\pi}{8}$$

(8)

$$V_R \geq \frac{c \times PRF}{16 \times f_c \times N_a}$$

(9)

where, V_R, PRF, f_c, f_s, N_a, c are the velocity of target in the range direction, the pulse repeated frequency, the center frequency, the sampling rate, the decimation ratio in the azimuth direction, and the speed of light, respectively.

On the other hand, in order to ensure the continuity of the target in the range direction, it is required that the moving distance of the target between two adjacent signals in the range direction is less than the sampling interval in the range direction:

$$\frac{2 \times V_R \times N_a}{PRF} \leq \frac{c \times N_R}{f_s}$$

(10)

$$V_R \leq \frac{c \times PRF \times N_R}{2 \times f_s \times N_a}$$

(11)

Therefore, the velocity of the target in the range direction should meet the following relationship:

$$\frac{c \times PRF}{16 \times f_c \times N_a} \leq V_R \leq \frac{c \times PRF \times N_R}{2 \times f_s \times N_a} \tag{12}$$

Accordingly, the system parameters are $PRF = 500$, $N_a = 20$, $N_R = 1$, $f_c = 1.26$ GHz, $f_s = 200$ MHz. For the proposed method, the velocity of the target in the range direction should meet the following condition:

$$0.37 \text{m/s} \leq V_R \leq 18.75 \text{ m/s} \tag{13}$$

Because of the differences in the structure and radar cross section of the moving targets, the scattering characteristics of the L-band signals with different polarizations are different. For the human, the body is structurally simpler, so the differences between the 3rd-order and the 4th-order central moment of the echoes in different polarization methods are small. For the non-motor vehicle, it is composed of many horizontal and vertical scatterers, and the radar cross section is relatively large compared to humans. Therefore, the echo signals in different polarizations have obvious differences in steepness and skewness.

We establish a feature plane consisting of a 3rd-order and 4th-order central moment, fusing the statistical features of three VH, VV, and HH polarimetric echoes to distinguish between pedestrians and non-motor targets.

4. Field Experiment

4.1. Radar Data Processing Flow

The moving target detection experiments were carried out; the developed L-band fully polarimetric radar was used to detect two types of moving targets, pedestrian and non-motor vehicle, and the proposed feature extraction method was applied to extract the statistical features of the two types of targets, respectively. It is noted that the non-motor vehicle target was a person pushing a bicycle during the detection experiment.
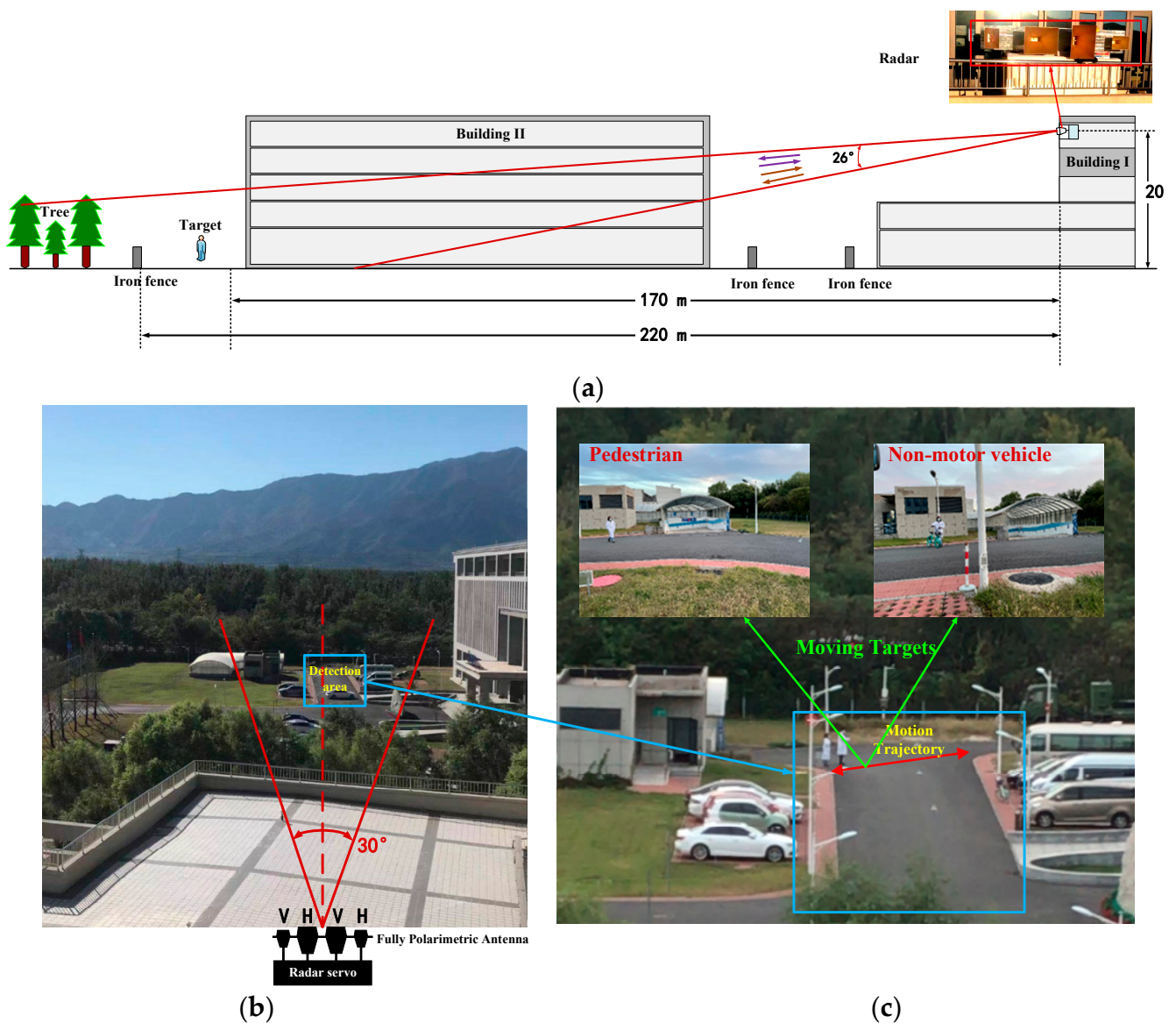
Figure 8 is the scene of the detection experiment. The L-band fully polarimetric radar was installed in building 1, with a height of 20 m above the ground, and the moving target to be detected was located between building II and the iron fence. The beam width of the antenna in the pitch direction was 26°, and the beam width of the antenna in the azimuth direction was 30°, covering 35–300 m in the range direction. The active area of the moving target was within the detection range of the radar, as illustrated in Figure 8a,b. Figure 8c is the schematic diagram of the moving target's range of motion and trajectory, as labelled by a red arrow. Figure 8c also demonstrates the motion process of two types of targets: pedestrian and non-motor vehicle. Both types of target move back and forth, and walk along the same straight line from the starting point to the end point.

4.2. Experiment Results

The L-band fully polarimetric radar data were collected during the movement of the two types of target, and the VH, VV, and HH radar data were processed, as described in Section 3. The experimental results of the pedestrian and non-vehicle are given below.
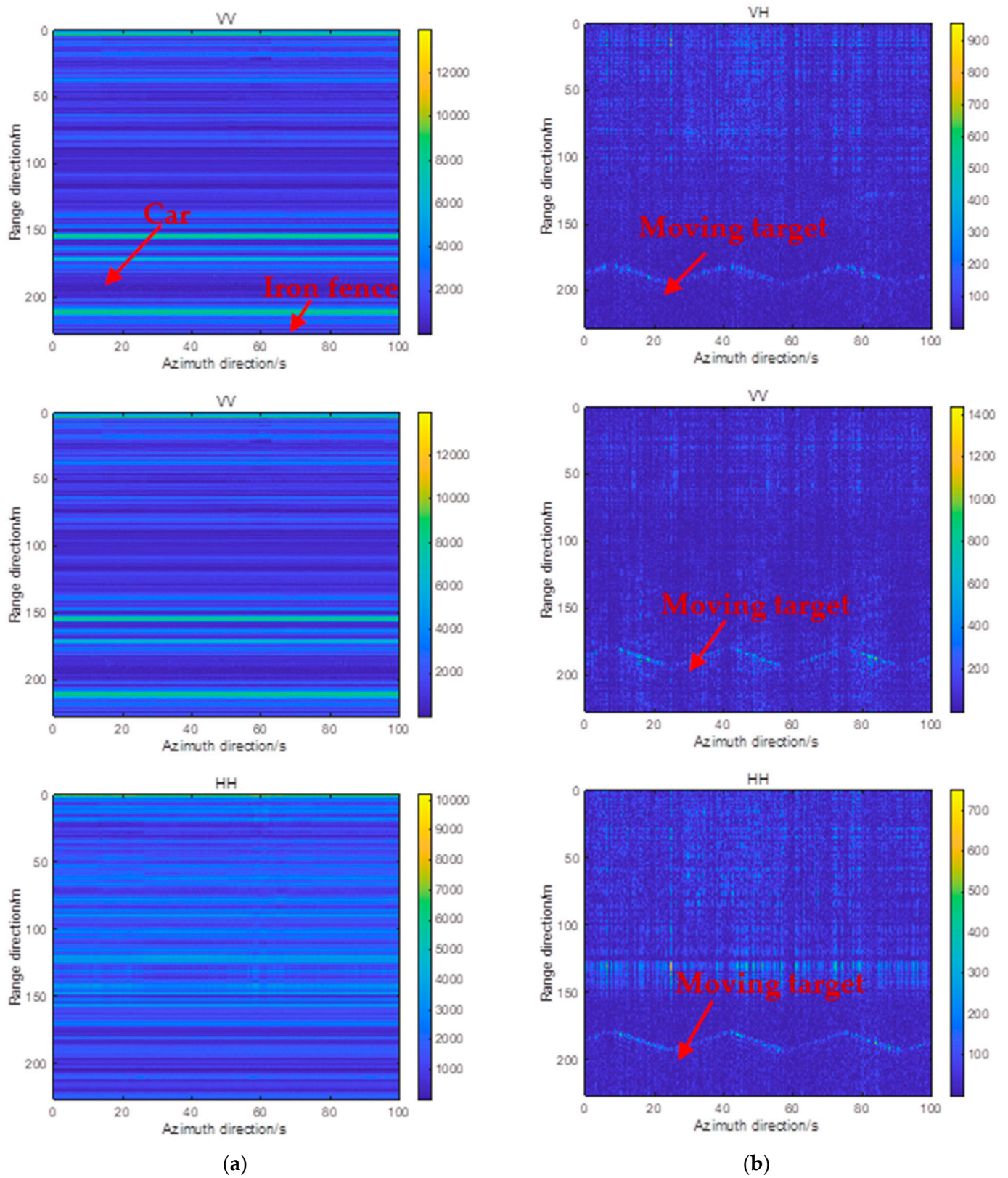
4.2.1. Detection Results for the Pedestrian

For the L-band fully polarimetric radar, the VH, VV, and HH radar echo are obtained as in Section 3.1. After orthogonal demodulation and pulse compression, the 2D range profiles for the pedestrian is given in Figure 9a. The trajectory of the pedestrian cannot be directly observed because there are multiple bright bars, which are caused by the strong scatters (such as a stationary car and an iron fence) in the detection scene. The background echoes are eliminated, as described in Section 3.2, and the outputs are listed in Figure 9b. It shows that the straight back and forth movement of the pedestrian is clear, which is consistent with the real trajectory.

Figure 8. Experimental scene. (**a**) The diagram of detection scene. (**b**) The real detection scenarios. (**c**) The area of the target movement.

Then, given the length of the sliding window, 22.5 m × 32 s, and that the sliding step was 0.04 s, the probability density curve of the echo intensity of the pedestrian inside the sliding window is estimated according to the method in Section 3.3. Figure 10 shows the sliding window and the 1000 probability density curves in 1000 windows for the pedestrian. The results indicate that there is no significant difference in the probability density curves of the intensity radar echo signal in the three different polarization modes. Finally, the 3rd- and 4th-order moments of the intensity of the radar echo in the VV, VH, HH polarization modes are calculated, according to Section 3.4. A feature plane, consisting of the 3rd-order and 4th-order central moment is created, and the statistical features of the three VH, VV, and HH echoes are fused, as illustrated in Figure 11, indicating that there is an overlap region in the distribution of the statistical features of the echo signals of the three polarization modes.

Figure 9. Two-dimensional range profiles of echo signal. (**a**) Before background removal. (**b**) After background removal.
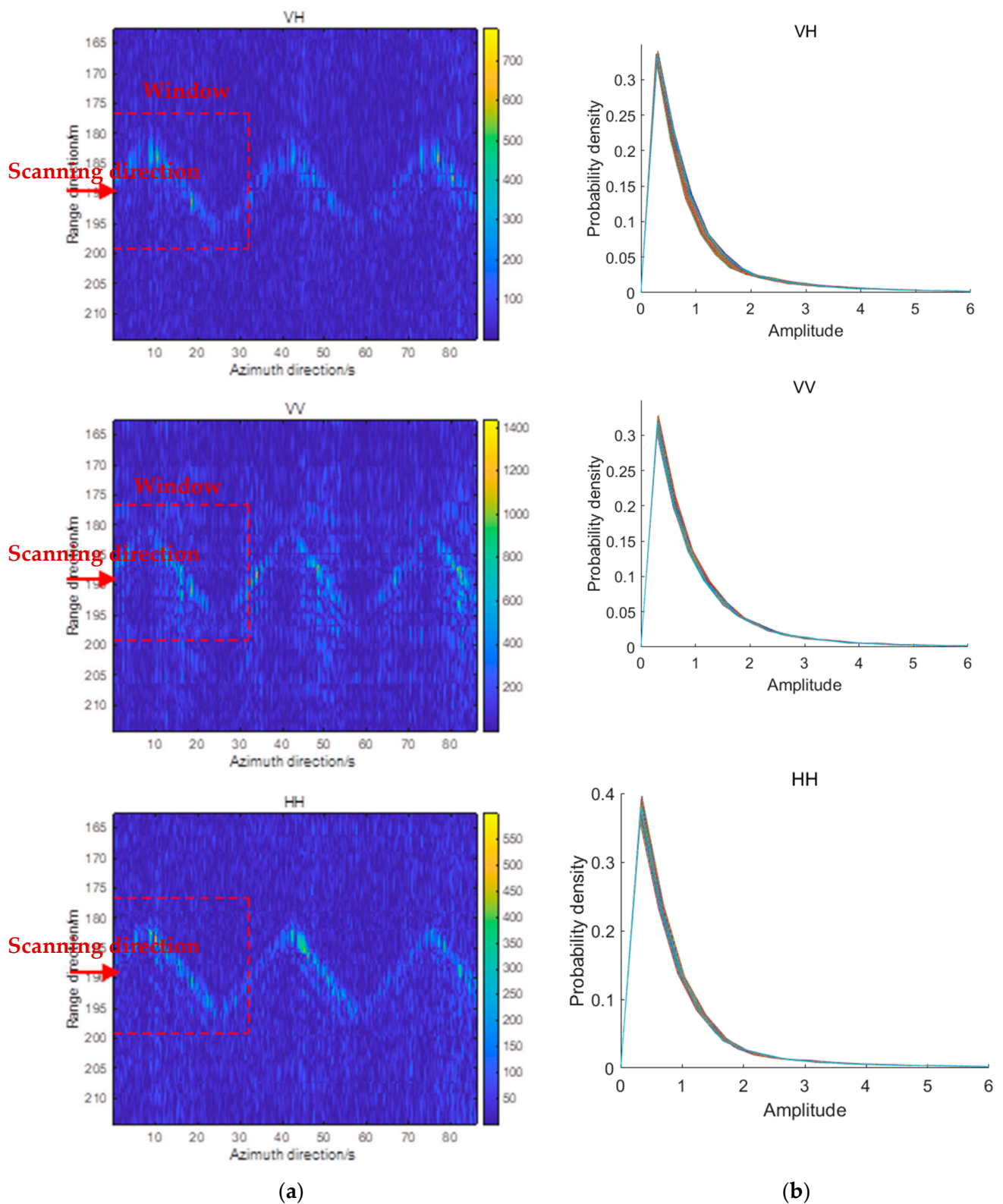
Figure 10. The probability density curves for the pedestrian. (**a**) 2D range compressed profile and its sampling window. (**b**) The curves of probability density function.
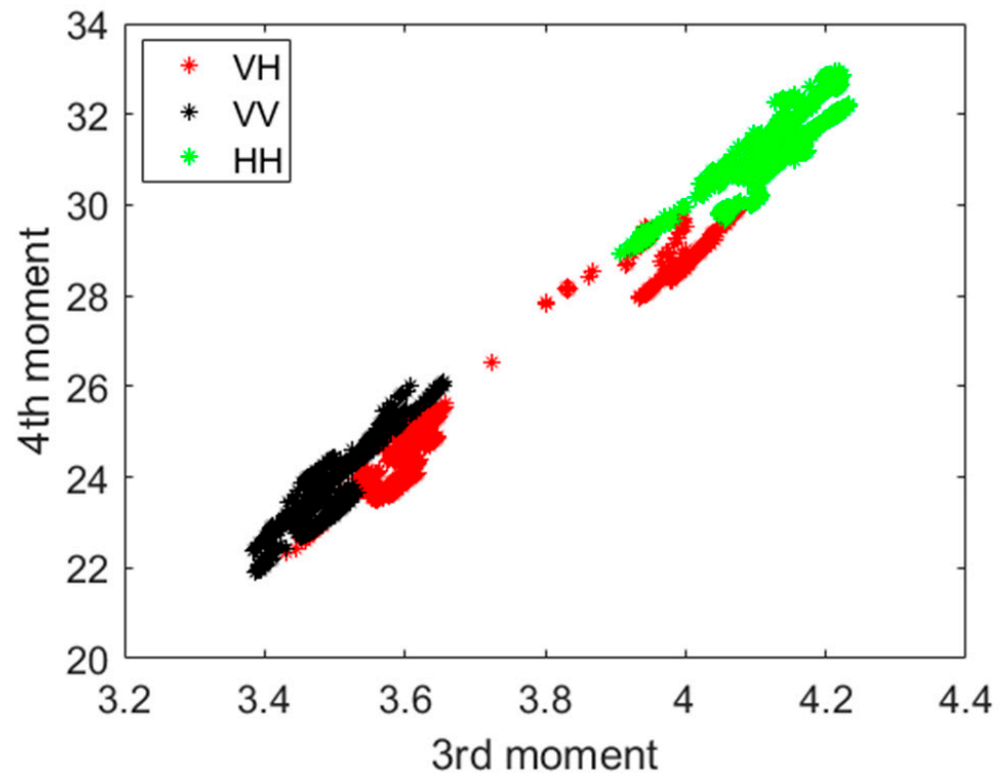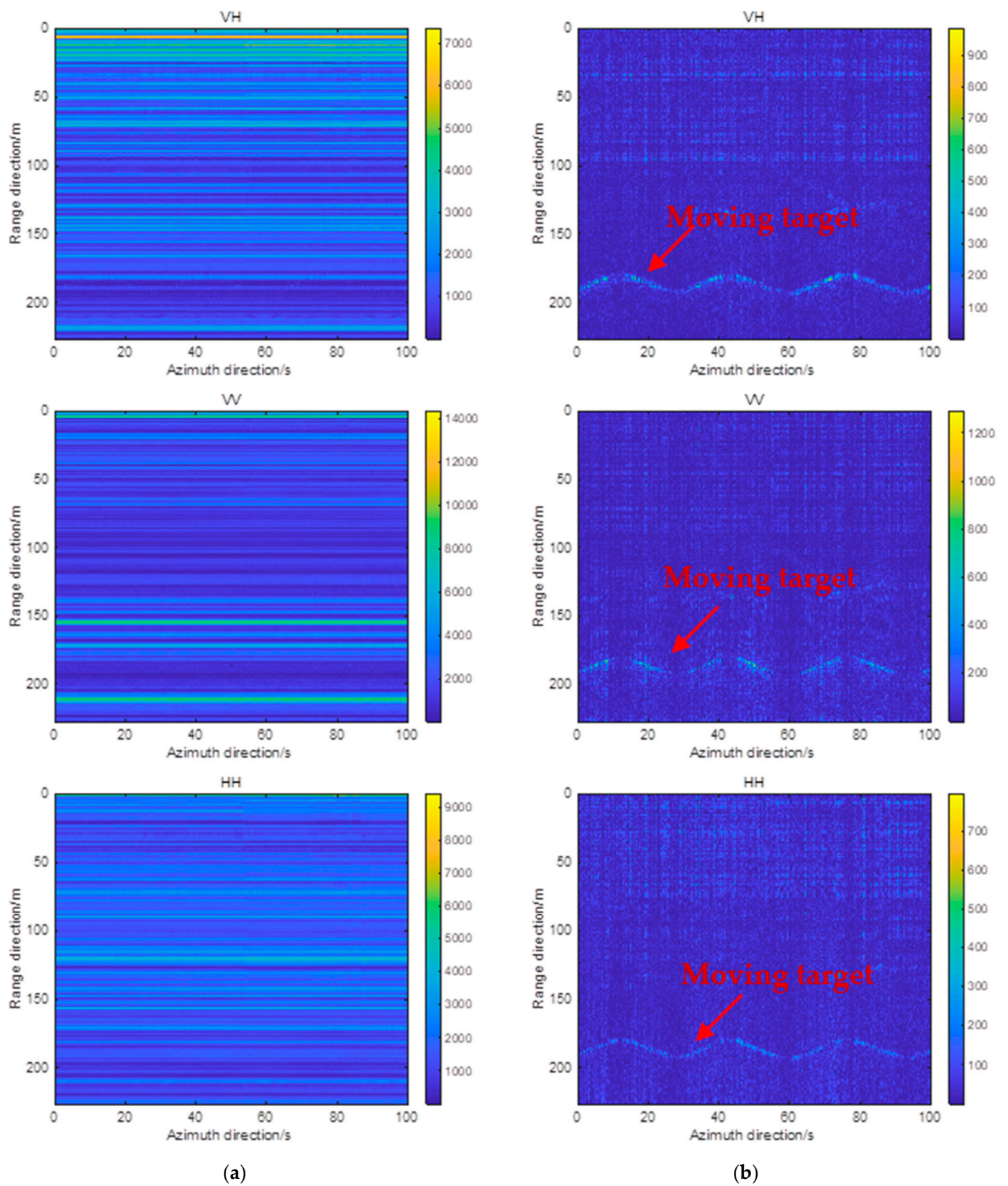
Figure 11. Statistical feature distribution of echo signals in three polarization modes for the pedestrian.

4.2.2. Detection Results for the Non-Motor Vehicle

For the non-motor vehicle, the processing of the fully polarimetric radar data is similar to the processing method in the pedestrian experiment. After orthogonal demodulation and pulse compression, the 2D range profiles of the VH, VV, and HH radar echoes are given in Figure 12a. As expected, the echo signals of the non-motor vehicles are buried by the echo signals generated by strong scatterers in the experimental scene, and the motion trajectories of non-motor vehicles cannot be directly observed from the range-Doppler plane. Then, the background echo is removed by the method described in Section 3.2. The 2D range profiles, after removing the interfering echoes, are shown in Figure 12b, indicating the trajectory of the non-motor vehicle; this matches up with the real movement of the non-motor vehicle.

Subsequently, 1000 sliding windows are set: the window size is 22.5 m × 32 s, the sliding step is 0.04 s, and the 1000 probability density curves of the echo intensity of the non-motor vehicle are estimated, according to the method described in Section 3.3, as illustrated in Figure 13. For the non-motor vehicles, the probability density curves of the radar echoes in VH, VV and HH polarization modes are obviously different in kurtosis and skewness. Finally, the 3rd- and 4th-order central moments of the intensity of the radar echo signals of the VV, VH, and HH polarization modes are calculated, according to Section 3.4. The feature plane of the 3rd- and 4th-order central moments is plotted in Figure 14. In accordance with the results of Figure 13, the echo signals of the three polarization modes are distributed in three different regions, with no overlap in the feature plane.

Figure 12. Two-dimensional range image of echo signal. (**a**) Before background removal. (**b**) After background removal.
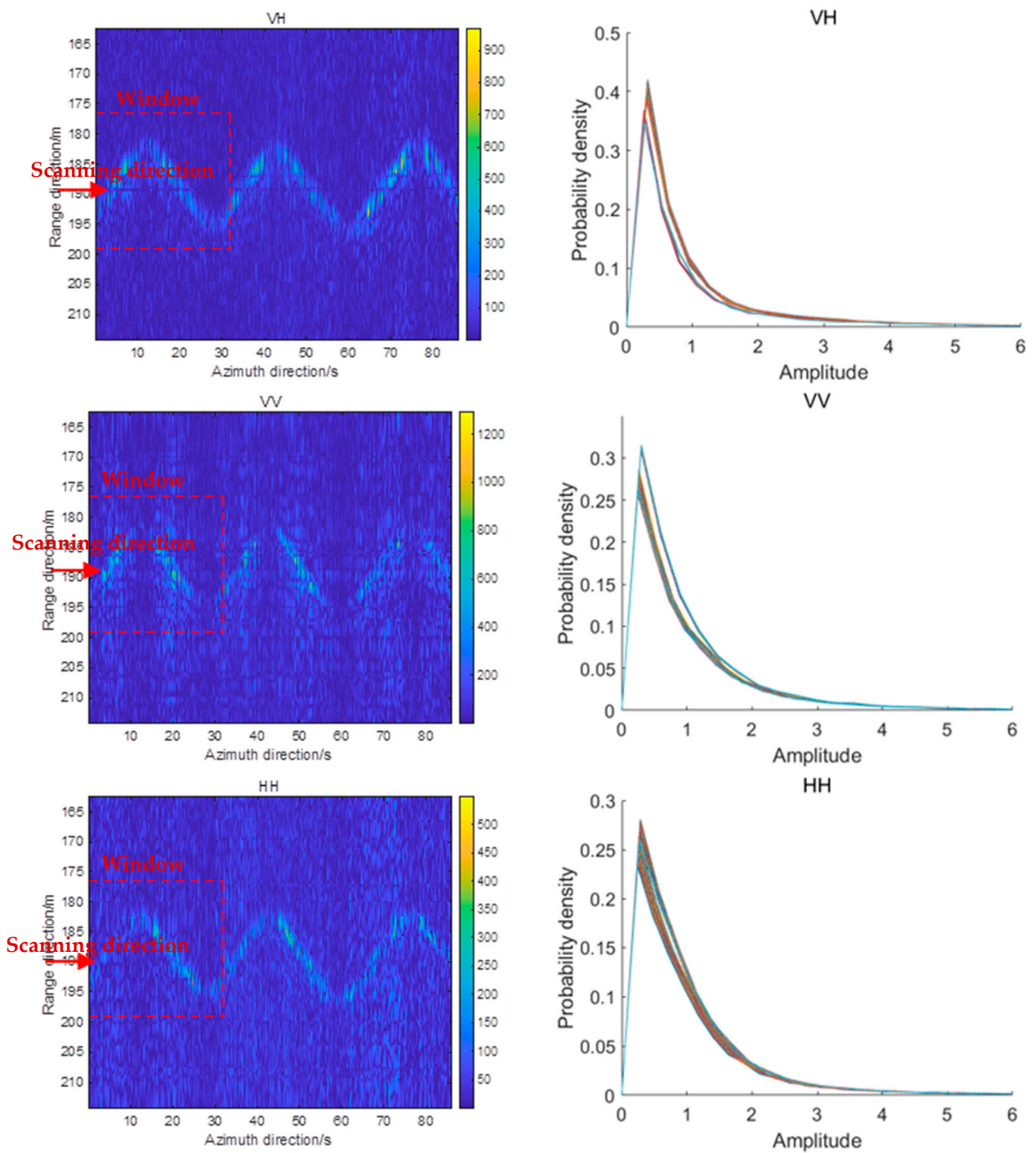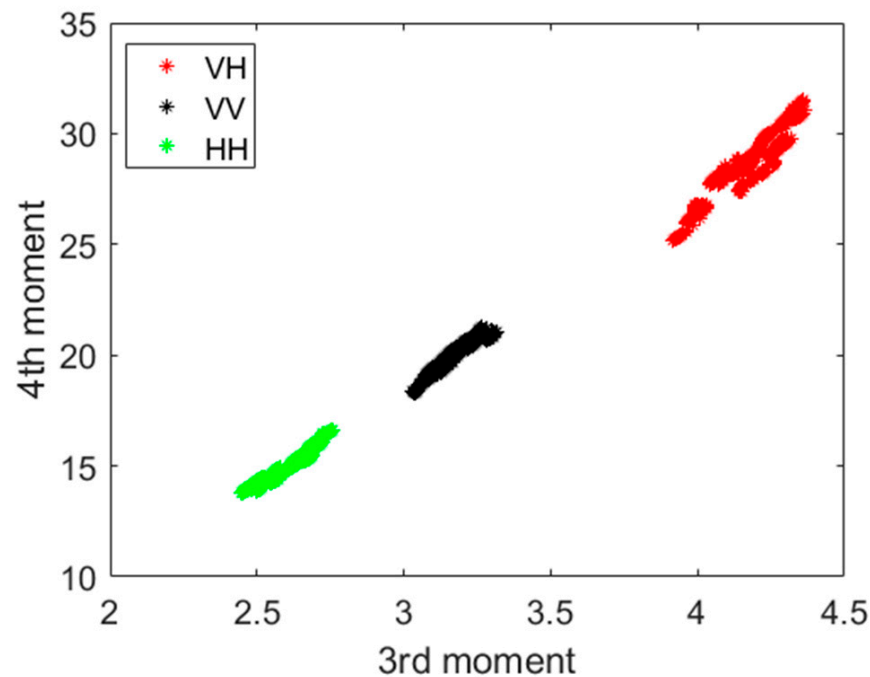
**Figure 13.** The probability density curves for the non-motor vehicle.

Figure 14. Statistical feature distribution of echo signals in three polarization modes for the non-motor vehicle.

5. Discussion

Comparing the feature plane in Figures 11 and 14, it can be seen that the statistical characteristics of the radar echo with full polarization in the L-band are significantly different for pedestrians and non-motor vehicles. The human body is structurally simpler. Therefore, for low-resolution L-band radar signals, the differences between the 3rd-order and the 4th-order central moment of the echoes in different polarization methods are small, and the VH, VV, and HH echoes appear to have overlapping distributions in the feature plane. Non-motor vehicles are structurally more complex, there are many horizontal and vertical scatterers, and the scattering cross-sectional area is relatively large compared to humans. Therefore, the echo signals for different polarizations have obvious differences in steepness and skewness, and appear to be distributed without overlap in the feature plane.

To further assess the stability of the proposed feature, we have conducted an additional set of detection experiments. The pedestrian target changes from a female to a male, the non-motor target is a man pushing a bicycle, and the other settings remain the same. Likewise, the fully polarimetric radar data, during the movement of the two types of targets, are processed separately, and the feature planes of the pedestrian and non-motor bike are shown in Figure 15. For pedestrians, there is an overlapping region of the three polarimetric radar signals, while for the non-motor vehicles, there is no overlapping region of the three polarimetric radar signals. It should be noted that, although the values of the 3rd-order and the 4th-order central moment of the same type of moving target are different, the distribution of the statistical features of the VH, VV, and HH polarization radar echoes is consistent in the feature plane. The experimental results verify that, based on the distribution characteristics of the full-polarization radar echo signal in the feature plane, pedestrians and non-motorized targets can be distinguished.
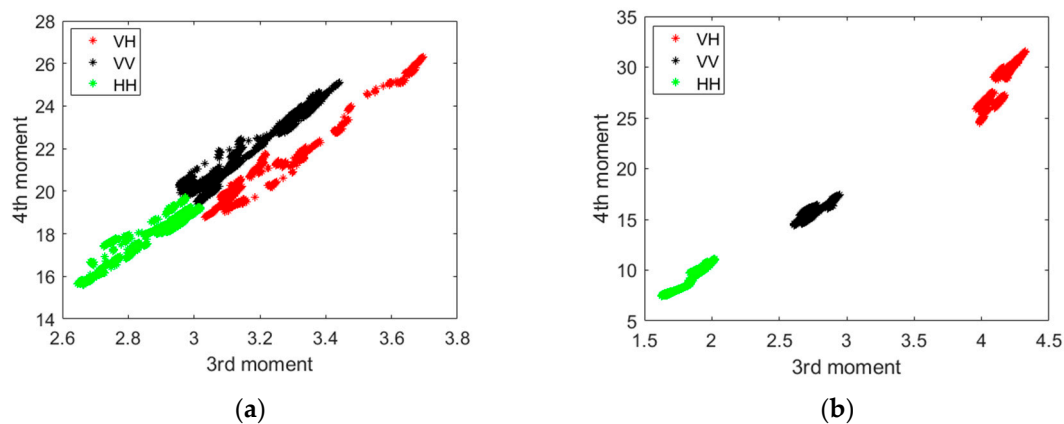
Figure 15. Statistical feature distribution of echo signals in three polarization modes. (**a**) Pedestrian. (**b**) Non-motor bike.

6. Conclusions

In this paper, we propose a novel feature extraction method for moving targets, based on the statistical characteristics of the echo amplitude of fully polarimetric radar echoes; field experiments are performed to evaluate the effectiveness and stability of this feature extraction algorithm for two types of moving target. The L-band fully polarimetric radar are developed, and the processing flow of the radar data is introduced. A 3rd- and 4th-order central moment feature plane is established, in which two types of moving targets, pedestrians and non-motorized vehicles, are able to be effectively distinguished according to the presence or absence of overlapping regions of the fully polarimetric signal in the feature plane. The proposed feature extraction method, based on statistical feature difference, has the advantage of being simple and robust, compared with the traditional feature extraction approach, based on imaging processing. In addition, the proposed statistical model is suitable for low-resolution radar data, which has low requirements for the radar system and has a significant value for engineering.

In subsequent studies, our team will increase the types of detected targets and the complexity of the detection scenes. Machine learning can be applied to achieve the automatic recognition of the target. We will try to establish echo databases of different types of target, based on the L-band full-polarization radars, and share the databases with research teams in need, free of charge. Any team interested in L-band fully polarimetric radar is warmly welcome to contact us and collaborate with us on research.

Author Contributions: Conceptualization, C.Z.; Data curation, Z.Z.; Formal analysis, C.Z.; Funding acquisition, Z.T. and Y.Z. (Ying Zhang); Investigation, X.L. and Y.Z. (Yao Zhang); Methodology, Z.X.; Project administration, S.J. and F.Y.; Software, L.Z.; Supervision, W.G.; Validation, X.L. and T.Z.; Visualization, Z.L.; Writing—original draft, C.Z. and Y.M. All authors have read and agreed to the published version of the manuscript.

Data Availability Statement: The data presented in this study are available on request from the corresponding author. The data are not publicly available due to [This data can only be used for scientific research and cannot be used for commercial applications].

Conflicts of Interest: The authors declare no conflict of interest.

References

1. Wang, Y.; Liu, Q.; Fathy, A.E. CW and pulse–Doppler radar processing based on FPGA for human sensing applications. *IEEE Trans. Geosci. Remote Sens.* **2012**, *51*, 3097–3107. [CrossRef]
2. Su, B.Y.; Ho, K.C.; Rantz, M.J.; Skuabic, M. Doppler radar fall activity detection using the wavelet transform. *IEEE Trans. Biomed. Eng.* **2014**, *62*, 865–875. [CrossRef] [PubMed]
3. Bilik, I.; Tabrikian, J.; Cohen, A. GMM-based target classification for ground surveillance Doppler radar. *IEEE Trans. Aerosp. Electron. Syst.* **2006**, *42*, 267–278. [CrossRef]
4. Wang, J.; Liu, Z.; Xie, R.; Ran, L. Radar HRRP target recognition based on dynamic learning with limited training data. *Remote Sens.* **2021**, *13*, 750. [CrossRef]
5. Novak, L.M.; Halversen, S.D.; Owirka, G.; Hiett, M. Effects of polarization and resolution on SAR ATR. *IEEE Trans. Aerosp. Electron. Syst.* **1997**, *33*, 102–116. [CrossRef]
6. Giusti, E.; Martorella, M.; Capria, A. Polarimetrically-persistent-scatterer-based automatic target recognition. *IEEE Trans. Geosci. Remote Sens.* **2011**, *49*, 4588–4599. [CrossRef]
7. Xiaodan, W.; Xu, Y. Target recognition of fully polarimetric HRRP based on H/A/α decomposition. *Syst. Eng. Electron.* **2013**, *35*, 2501–2506.
8. Yuxi, Z.; Xiaodan, W.; Xu, Y.; Lei, L. Approach of radar target recognition based on multiple polarization features fusion. *Comput. Sci.* **2012**, *39*, 208–210.
9. Ding, L.; Hongwei, L. Radar target classification based on some invariant properties of the polarization. *Radar Sci. Technol.* **2013**, *11*, 165–172.
10. Wang, P.; Wang, L.; Leung, H.; Zhang, G. Super-resolution mapping based on spatial–spectral correlation for spectral imagery. *IEEE Trans. Geosci. Remote Sens.* **2020**, *59*, 2256–2268. [CrossRef]
11. Lu, J.; Li, J.; Chen, G.; Zhao, L.; Xiong, B.; Kuang, G. Improving pixel-based change detection accuracy using an object-based approach in multitemporal SAR flood images. *IEEE J. Sel. Top. Appl. Earth Obs. Remote Sens.* **2015**, *8*, 3486–3496. [CrossRef]
12. Jian, W.; Yongguang, C.; Dahai, D.; Chen, S.; Wang, X. Target recognition for polarimetric HRRP based on fast density search clustering method. *J. Electron. Inf. Technol.* **2016**, *38*, 2461–2467.
13. Shengqi, L.; Jiemin, H. Full-polarization radar target recognition of multitask compressive sensing. *J. Natl. Univ. Def. Technol.* **2017**, *39*, 144–150.
14. Xia, Z.; Zhang, Q.; Ye, S.; Wang, Y.; Chen, C.; Yin, H.; Fang, G. A novel low-frequency coded ground penetrating radar for deep detection. *IEICE Electron. Expr.* **2015**, *12*, 20150200. [CrossRef]
15. Xia, Z.; Fang, G.; Xia, Z.; Ye, S.; Zhang, Q.; Chen, C.; Yin, H. A novel handheld pseudo random coded UWB radar for human sensing applications. *IEICE Electron. Expr.* **2014**, *11*, 20140981. [CrossRef]
16. Xia, Z.; Jin, S.; Yue, F.; Yang, J.; Zhang, Q.; Zhao, Z.; Zhang, C.; Gao, W.; Zhang, T.; Zhang, Y.; et al. A Novel Space-Borne High-Resolution SAR System with the Non-Uniform Hybrid Sampling Technology for Space Targets Imaging. *Appl. Sci.* **2022**, *12*, 4848. [CrossRef]
17. Staderini, E.M. UWB radars in medicine. *IEEE Aerosp. Electron. Syst. Mag.* **2002**, *17*, 13–18.
18. Zhang, C.; Mori, S.; Hirata, S.; Hachiya, H. Examination of optimal moments as input parameters for evaluation of liver fibrosis based on multi-Rayleigh model. *Jpn. J. Appl. Phys.* **2018**, *57*, 07LF27. [CrossRef]
19. Igarashi, Y.; Yamaguchi, T.; Hachiya, H. Stability of Quantitative Evaluation Method of Liver Fibrosis Using Amplitude Distribution Model of Fibrotic Liver. *Jpn. J. Appl. Phys.* **2011**, *50*, 07HF17. [CrossRef]
20. Zhang, C.; Hirata, S.; Hachiya, H. Accuracy evaluation of quantitative diagnosis method of liver fibrosis based on multi-Rayleigh model using optimal combination of input moments. *Jpn. J. Appl. Phys.* **2020**, *59*, SKKE27. [CrossRef]